Spatiotemporal scales of dynamical functional networks – using whole-brain modelling to identify the optimal resolution

Xenia Kobeleva [1 2 3], Ane López-González [2], Morten Kringelbach [4 5], Gustavo Deco [2, 6, 7, 8]

(1) Department of Neurology, University of Bonn, Venusberg-Campus 1, 53127 Bonn, Germany

(2) Center for Brain and Cognition, Computational Neuroscience Group, Universitat Pompeu Fabra, 08018 Barcelona, Spain

(3) German Center for Neurodegenerative Diseases (DZNE), Bonn, Venusberg-Campus 1, 53127 Bonn, Germany

(4) Department of Psychiatry, University of Oxford, Oxford OX3 7JX, United Kingdom

(5) Center for Music in the Brain, Department of Clinical Medicine, Aarhus University, 8000 Aarhus, Denmark

(6) Institució Catalana de la Recerca i Estudis Avançats (ICREA), 08010 Barcelona, Spain

(7) Department of Neuropsychology, Max Planck Institute for Human Cognitive and Brain Sciences, 04103 Leipzig, Germany

(8) School of Psychological Sciences, Monash University, Melbourne, Clayton, VIC 3800, Australia

Corresponding author: Dr. Xenia Kobeleva, Department of Neurology, University of Bonn, Venusberg-Campus 1, 53127 Bonn, Germany; email: xenia.eaynt@gmail.com

Abstract

The brain can rapidly process and transfer information between cortical brain networks by dynamically transitioning between brain states. Here we study the switching activity between functional brain networks that have been estimated at various spatial scales from n = 100 to n = 1000 using resting-state fMRI data. We also generate timeseries at different temporal scales from milliseconds to seconds using whole-brain modelling. We calculate the entropy of switching activity between functional brain networks which represents the richness of the dynamical repertoire. We provide evidence that the entropy of functional network occurrence follows an inverted U-shaped curve with a maximum at a spatial scale between 200 and 300 regions and at a temporal scale of 200 milliseconds.

Keywords: neuroscience, modelling, spatiotemporal, brain dynamics

Introduction

The brain can rapidly process and adapt to new information through transitioning between multiple cognitive states. There has been substantial interest in neuroimaging research to better understand how the brain executes these rapid transitions between cognitive states from an anatomical and functional perspective, e.g. through investigating *brain dynamics* that describe the changes of brain activity and brain network connectivity over time and space (Stitt et al. 2017). To derive metrics of brain dynamics, researchers have to decide on the temporal scale (meaning the sampling rate) and the spatial scale (meaning the spatial resolution) of the data. Whereas lower spatiotemporal scales (i.e., more coarse resolutions) are associated with loss of relevant information, higher spatiotemporal scales (i.e., finer resolutions) lead to increases of unwanted noise and enhanced computational complexity and inefficiencies. In practice, current brain dynamics studies vary widely in their choice of spatiotemporal scales. Therefore, the description of the brain dynamics remains a challenge to neuroscientific researchers not only due to the arbitrary choice of experimental parameters that massively influence the resulting metrics of brain dynamics. In fact, the fundamental question at which spatiotemporal scale the brain intrinsically transitions between functional states has so far remained unanswered.

Several studies have performed comparisons between spatial scales. In these studies, spatial scales and parcellation techniques were compared in regard to various metrics, such as reproducibility of resulting networks, agreement with other modalities such as anatomical connectivity, and their effect on prediction accuracy of neuropsychiatric conditions (Dadi et al. 2019; Arslan et al. 2018; Messé 2019). For instance, Proix et al. (2016) investigated the effect of spatial scale on information content in a model of brain dynamics by decomposing the simulated timeseries using a principle component analysis and found an optimum at around 140 regions. While all these studies have significantly contributed to our fundamental understanding of how different spatial scales affect the analyses of brain dynamics, they only focus on identifying the optimal spatial scale in isolation without taking into account the temporal scale. In empirical research practice, however, every measurement in brain dynamics features both a spatial and a temporal scale.

Experimental comparisons between temporal scales would require a comparison of several studies using different neuroimaging modalities, but there is still a lack of robust translations of brain dynamics metrics between different modalities. For this question dynamical whole-brain network models offer a practical solution to contrast different temporal scales. A previous study using a generative whole-brain network model compared brain dynamics between different temporal scales (2019) a temporal scale of 200 milliseconds captures the most relevant information on brain dynamics by calculating the entropy of switching between functional brain networks. As this study focused on the assessment of the optimal temporal

scale, it was not considered whether the optimum of temporal scale would be contingent on the spatial scale.

In this study, we address the previously neglected link between spatial and temporal scales in their optimal values for brain dynamics analyses by adding a temporal scale to our analyses of optimal spatial scales. We seek to provide an assessment of the optimal, integrated spatiotemporal scale at which the brain performs dynamical state reconfigurations. In addition, in identifying potential interaction effects between optimal spatial and temporal scales, we aim at reducing researchers' uncertainty inherent in choosing appropriate neuroimaging modalities and parcellation techniques. Thus, our study should not only have implications for a better understanding of the relevant spatial and temporal scale of dynamical reconfiguration of brain networks over time, but also contributes to the robustness and sensitivity of brain dynamics metrics as potential biomarkers of neuropsychiatric diseases.

To achieve this goal, we explore the switching behavior of spatial networks at spatial scales from 100 to 900 regions both in empirical timeseries extracted from resting-state fMRI with fixed temporal scales as well as in simulated timeseries with various temporal scales from milliseconds to seconds. We determine the relevant spatiotemporal scale by comparing the entropy of the switching activity, so that it maximizes the relevant informational content of spatiotemporal networks. In the discussion of our results, we derive recommendations for researchers, highlighting our finding that the relevant spatial scale for analyses of brain dynamics lies at 200-300 regions and at a optimal temporal scale of 200 milliseconds and thus contribute to an empirical basis of relevant parameters for studies of brain dynamics.

Methods

Data acquisition and preprocessing

We used resting state functional data from 94 of 100 unrelated subjects of the Human Connectome Project (HCP; Van Essen et al. 2013); six subjects were due to methodological reasons as FC matrices consisted of at least one N/A row in one of the higher parcellations. We further chose one of the four available resting-state fMRI scans of about 15 minutes duration (TR of 0.72 sec). During fMRI acquisition, subjects were instructed to keep their eyes open while looking at a fixation cross. A full description of the imaging parameters and minimal preprocessing pipeline can be found in Glasser et al. (2013). In short, after correction for motion, gradient and susceptibility distortions the fMRI data was aligned to an anatomical image. The aligned functional image was then corrected for intensity bias, demeaned and projected to a common surface space, which resulted in a cifti-file.

We also employed an independent dataset from the enhanced NKI Rockland study (Nooner et al. 2012). We chose fMRI data (TR = 2.0 sec) from the first 50 subjects who participated in a 10-minute resting-state fMRI scan with their eyes open and a fixation cross. We used the

preprocessed fMRI data (see McDonald et al. 2017 for preprocessing details). Briefly, fMRI data was corrected for slice timing and coregistered to the anatomical scan. Subsequently, we performed a nuisance variable regression and the data was transformed into MNI space and smoothed using a 6mm FWHM kernel.

Both studies were approved by the local ethical committees and informed consent was obtained from all subjects.

All fMRI data was filtered between 0.1 and 0.01 Hz to retain the relevant frequency range for further analyses. We obtain structural and functional matrices in different spatial scales using the Schaefer parcellation, which optimizes local gradient and global similarity measures of the fMRI signal in various spatial scales ranging from 100 to 1000 regions (Schaefer et al. 2018). In both fMRI datasets timeseries were extracted with the help of the connectome workbench for the HCP data and *fslmeants* for the NKI data. We correlated the timeseries of all regions with each other using the pairwise Pearson correlations and normalized the resulting r-values using the Fisher's transform.

To make our analyses more robust, we performed several iterations of the model fitting to the empirical data. To do so, the HCP fMRI data was split into two groups. The first 30 subjects were used for model fitting (see below). A subset of 10 subjects out of the second group was randomly selected in 20 iterations and their timeseries were concatenated for the estimation of the empirical spatiotemporal networks. The NKI dataset was used for validation of the model fitting.

To create a structural connectivity matrix as a basis for the whole-brain model, we generated a normative structural connectome depicting the fiber density in the required spatial scales, based on 32 HCP subjects (Horn et al. 2017; Setsompop et al. 2013) using the Lead-DBS toolbox version 2.0 (Horn et al. 2018). Structural matrices were constructed in the same spatial scales as the functional data.

Whole-brain modelling

The use of fMRI signals would normally limit our study in the temporal dimension. To overcome this shortcoming, we use a whole-brain model which allows us simulate data in varying timescales from milliseconds to seconds, while preserving the statistics of the empirical signals. We create a dynamic mean field model, which is conceptually based on pools of neurons that contain excitatory and inhibitory neurons. These neurons emit spontaneous neuronal noise which is broadcasted to the rest of the network. We further assume that multiple pools of neurons interact, as given by the interactions of the structural connectome (Deco et al. 2014). These assumptions are implemented through a modified DMF model based on the original reduction first proposed by Wong and Wang (2006).

A summary of the individual steps that were taken to create the model can be found in Figure 1. In the model used in this study, NMDA receptors represent excitatory connections and GABA-A receptors represent inhibitory connections. Additionally, there are long-range connections mediated by AMPA receptors. Inhibitory sub-populations communicate reciprocally with excitatory sub-populations on a local level. Excitatory sub-populations are additionally linked with to other excitatory sub-populations via long-range connections. The weights of the links are based on the fiber density weights given by the structural connectome, scaled by a global scaling factor G.

We adjusted the dynamical parameters of the model so that excitatory subpopulations have a spontaneous firing rate of 3 Hz and inhibitory subpopulations have a rate of 9 Hz. The weight of feedback inhibition is adjusted for each excitatory subpopulation to obtain a firing rate of about 3 Hz, using a regulatory mechanism called Feedback Inhibition Control (Deco et al. 2014).

The resulting neuronal signal is transformed into a simulated fMRI BOLD-signal by employing the Balloon-Windkessel hemodynamic model (Stephan et al. 2007), which depicts the transduction of the sum of inhibitory and excitatory neural activity to perfusion changes. To focus on the functionally relevant frequency range, we band-pass filtered the BOLD signals between 0.1 and 0.01 Hz (Glerean et al. 2012; Achard et al. 2006).

We perform the fitting to the empirical signals using the global coupling parameter, which adjusts the coupling of the connections so that the fit of simulated brain dynamics to the empirical brain dynamics is maximized. The global scaling parameter is the only parameter that is adjusted according to the empirical data using model fitting (see below).

The fitting of the data was performed by adjusting the global scaling factor to improve the fit to three different metrics; average functional connectivity (FC), the Kuramoto synchronization index, and dynamical functional connectivity (DFC) (below). Each of these metrics represents different properties of empirical signal, so performing a good fitting of the three measures ensures maintaining biologically plausible signal statistics in the simulated timeseries. Using this model, we created simulated BOLD data of 10 subjects.

To obtain robust fitting values, we performed 10 iterations of the fitting of 10 randomly chosen subsets from the HCP dataset and validate the fitting using the NKI dataset.

Dynamical measures used for the fitting:

Average FC: The average FC was created by correlating BOLD signals pairwise over the complete acquisition period using Pearson correlations. We compared the empirical and simulated FC using the Pearson correlation.

Kuramoto synchronization index: The synchronization index measures the global level of phase synchronization. It is calculated as the mean of the Kuramoto order parameter R(t) across time, which depicts the average phase φ of the system across *n* regions.

$$R(t) = \left| \sum_{k=1}^{n} e^{i\varphi_k(t)} \right|_{n} \quad (1)$$

We extracted the Kuramoto synchronization index by detrending the filtered fMRI timeseries and calculating the phases of the timeseries of each region using the Hilbert transform. We calculated the differences between empirical and simulated Kuramoto synchronization index, that has been previously proven to be suitable to define the dynamical working point of dynamical whole-brain models (Deco et al. 2017).

DFC: We evaluated the temporal dependencies of spatial correlation using the DFC. We first extracted the difference of phases between regions using the cosine, resulting in a similarity matrix representation. Subsequently, we divided the regional phase differences into time windows of about two seconds and computed the correlations between the phase similarity matrices between time windows, which resulted in a representation of spatiotemporal fluctuations of phases.

Extraction of spatiotemporal networks using ICA and calculation of entropy

To retrieve different temporal scales from the simulated BOLD data in the range of milliseconds to seconds, the timeseries were binned by averaging the signals in windows of the width of the according timescale. The temporal scale of the empirical data was determined by the TR (HCP: 720 ms, NKI: 2000 ms). We then extracted spacetime motifs from the empirical and simulated timeseries. To reduce dimensionality of the data, the timeseries were binarized using the point-process binarization algorithm for BOLD signals (Tagliazucchi et al. 2012).

To estimate the number of relevant spatiotemporal networks, we applied an adaptation of an eigenvalue analysis for assessing the statistical significance of resulting networks (Peyrache et al. 2010), as introduced by Lopes-dos-Santos, Ribeiro, and Tort (2013). This method finds the number of principal components within the event matrix that have significantly larger eigenvalues compared to a normal random matrix as introduced by Marčenko and Pastur (1967). After determining the number of relevant spatiotemporal networks, we extracted these networks by applying an ICA to the binarized event matrix, resulting in a matrix of spatiotemporal networks with *n* brain regions and *c* independent components.

Lastly, we evaluated the resulting temporal evolution of spatiotemporal networks by tracking their activity over time (see Figure 2B). Through projection of the binarized event matrix onto the network matrix, the similarity between each network and the whole-brain activity at each

time point could be assessed. This resulted in an activity matrix of the temporal activity of each network:

$$A_{cb} = e_b^T P_c e_b \quad (2)$$

with e being the event matrix n (with dimension number of regions x binned time points) and the projection matrix P_c defined as:

$$P_c = \vec{w}_c \otimes \vec{w}_c^T = \vec{w}_c \vec{w}_c^T \quad (3)$$

where $\otimes$ is the outer product operator and $\vec{w}_c$ one of the extracted ICA components from the event matrix.

By calculating the ratio of activity of each network in relation to overall activity, we were able to retrieve a probability of each network:

$$p(c) = \sum_b A_{cb} \Big/ \sum_{c,b} A_{cb} \quad (4)$$

Using these probabilities, we computed the entropy of occurrence of each network, representing the diversity of switching activity between spacetime networks.

$$H = -\sum_c p(c) \log(p(c)) \quad (5)$$

The entropy was then normalized for the resulting number of networks.

Results

We aimed to define the optimal spatiotemporal scale that captured the most relevant information about the temporal evolution of functional networks. We extracted timeseries at different parcellations at different spatial scales (from n = 100 to n = 1000) in the empirical data. Furthermore, we created a dynamic mean-field model to create timeseries at various temporal scales from milliseconds to seconds (Figure 1). Using both simulated and empirical timeseries, we explored the probability of occurrence of meaningful functional spatiotemporal networks over time. We calculated the entropy of these probabilities' occurrence of each network as a proxy of the diversity of switching activity between spatiotemporal networks (Figure 2).

Validation of the whole-brain model

The dynamic mean field model is a neuronal model that recreates inhibitory and excitatory synaptic dynamics (including AMPA, GABA and NMDA receptors) following the structure given by the underlying anatomical connectivity. By using the steps detailed in Figure 1 and following the constraints of anatomical connectivity as provided by the normative structural connectome, we were able to create realistic neuronal timeseries at the scale of milliseconds to seconds

using the dynamic mean field model. To ensure the robustness of the model, we fitted the resulting simulated BOLD timeseries to the empirical BOLD timeseries from two independent datasets using the DFC and the global synchronization level (see Figure 3). For each spatial scale, the fitting resulted in two optima at a global coupling value G between 1.55 and 1.85 and at between 2.2 and 2.5. We chose the first peak to create the mean-field model, as using the first peak resulted in an adequate representation of the empirical dataset with comparable numbers of spatiotemporal networks. In contrast, the second peak had much lower numbers of spatiotemporal networks (e.g. 5 networks at a spatial scale of 100 regions).

Entropy of evolution of spatiotemporal networks

The evolution of spatiotemporal networks over time and their probabilities of occurrence allow us to estimate the richness of the dynamical repertoire at various spatiotemporal scales from a probabilistic perspective. In Figure 4, we display the entropy of spatiotemporal networks as a function of the spatial and temporal scale in the empirical and simulated dataset. As the number of networks was contingent on the spatial scale used, we corrected the entropy for the logarithm of the number of networks. We discovered an inverted U-shape form of the entropy both of the empirical and simulated timeseries, based on calculating the entropy as a function of probability of spatiotemporal networks across time. Regarding the spatial scale, the maximal entropy was found on a scale between 200 and 300 regions, but with only a minor decrease at scales with 100 or 400 regions. At scales above 400 regions, we observed a drop in entropy with a further decrease with increasing numbers of regions. Regarding the temporal scale, the highest entropy was to be found at 200 ms. Taking both scales into account, the highest level of entropy could be found at a temporal scale of 200 ms with similar values of spatial scales between 100 to 300 regions. At increasing temporal scales at the range of seconds, the highest entropy was achieved with 300 regions and to a slightly smaller degree with 100 and 200 regions.

Spatiotemporal networks across spatial and temporal scales

Figure 2 summarizes the workflow to create the spatiotemporal networks from the binned data across different spatial and temporal scales. Using the empirical and simulated data, we determined the number of networks by counting the number of eigenvalues above the maximum of the eigenvalues, as given by the null hypothesis distribution based on random matrix theory as given by the Marčenko–Pastur distribution. To ensure that the simulated timeseries captured the relevant characteristics of the empirical data, we also compared the number of resulting networks between the empirical and simulated timeseries, which followed a similar trend. We observed a linear increase of the number of networks at an increasing spatial scale in both empirical and simulated datasets, starting with an average of 13.72

(empirical) vs. 16.0 (simulated) networks at a scale of n = 100 to over 22.29 (empirical) vs. 27.0 (simulated) networks at scale of n = 200 until up to an average 67.79 (empirical) networks at a scale of n = 900.

An example depicting the spatial distribution of the resulting empirical and simulated spatiotemporal networks at the spatial scale of n = 200 with associated probabilities of each network can be found in Figure 5. At the lower spatial scales (e.g. n = 200), the networks resembled classical resting state networks. At higher scales, more networks arose—with a significant proportion of the networks having a low probability of occurrence (below 1%, as can be seen for a network with n = 900 in supplementary figure S1).

Discussion

In this study, we investigated the most relevant optimal spatiotemporal scale at which fundamental macroscopic dynamical processes within the brain take place. We followed functional spatiotemporal networks over time not only at different spatial scales, but through the use of a dynamic mean-field model also at fine-grained temporal scales from milliseconds to seconds. Across empirical and simulated functional timeseries, we generated evidence that the entropy of network occurrence followed an inverted U-shaped curve with a maximum at a spatial scale between 200 and 300 regions and at a temporal scale of 200 milliseconds.

Our findings are consistent with the study by Proix et al. (2016), who investigated the information content of the effect of a perturbation paradigm on functional connectivity in a dynamical model, and who also found an inverted U-shaped function with an optimum of around 140 regions. Most other prior studies rather focused on the effect of spatial scales more from an analytical point view in regard to reproducibility (Arslan et al. 2018) or prediction accuracy (Dadi et al. 2019; Abraham et al. 2017) with optimal values between 100 and 150 regions; however, our focus was more general in regard to the functionally relevant scale of brain dynamics. Nonetheless, even when considering prediction accuracy or reproducibility more broadly (i.e., as measures of relevant information content), our findings on entropy of brain dynamics are complementary to these measures. Moreover, we join the argument of these studies that although choosing a higher number of regions for analyses of brain dynamics adds complexity to the representation of the dynamical repertoire of the human brain, this additional information is not necessarily more relevant. As shown by our analyses, additional complexity as given by increased spatiotemporal scales can be detrimental—not only increasing the computational cost of the analysis, but also adding irrelevant and noisy signals to the analyses.

Our findings have several implications for future research of brain dynamics. First, we were able to reproduce the finding of the optimal temporal scale of 200 ms (Deco, Cruzat, and Kringelbach 2019). Our findings reflect experimental results of temporal dynamics of conscious

processes that operate at similar temporal scales and typically involve a rapid temporal sequence of information stabilization and transfer (Mai, Grootswagers, and Carlson 2019; Wutz et al. 2014; Salti et al. 2015). On top of that, our study shows that the optimal temporal scale represents a general rule and is not contingent on the spatial scale used. For researchers aiming to extract the most relevant information content in their analyses of brain dynamics, we therefore advise to either use neuroimaging modalities operating at this optimal temporal scale (e.g. MEG or EEG) or augment their analyses with whole-brain modelling, which allows to take other temporal scales into consideration. Second, our study provides an empirical basis for neuroimaging studies using dimensionality reduction techniques while preserving the most relevant information of brain dynamics. This is because we provided evidence that a spatial scale between 200 and 300 regions is sufficient to capture the most relevant information on macroscopic brain dynamics. While lower scales may be associated with a loss of information, higher spatial scales introduce irrelevant and noisy functional networks.

Limitations and outlook

We used independent component analysis (ICA) to derive functional networks at different scales. As any other method, ICA is not free of underlying assumptions and especially assumes maximal spatial independence of the networks (Jutten and Herault 1991). Future studies could consider additional analyses using other metrics such as network measures or apply emerging techniques that specifically consider the change of spatial composition of functional networks over time (Geniesse et al. 2019). As Arslan et al. (2018) and Hilger et al. (2020) demonstrated in their studies that network measures of integration and segregation are largely altered by the spatial scale, appropriate correction techniques should be used for such analyses across scales. In regard to the parcellation used, we used the Schaefer parcellation for our analyses across scales, which is ideal for cross-study comparisons at increasing spatial scales because it is offers fine-grained parcellations at various spatial scales in both MNI and surface space. Future studies could also consider other fine-grained parcellations (Hagmann et al. 2008) and consider comparing the contribution of cortical versus subcortical regions on the dynamical repertoire of the brain which might operate at other temporal scales during subconscious processes (Ji et al. 2019).

Overall, our results suggest that the brain operates at an optimum of about 200 – 300 regions and a timescale of 200 milliseconds. We therefore provide a framework for a general understanding of spatiotemporal dynamics of brain processing, which could be an inspiration for future studies to harmonize spatiotemporal scales.

Acknowledgements

X. K. was supported by a short-term fellowship of the European Molecular Biology Organization (n. 7366) and by an InEurope fellowship of the International Brain Research Organization. G.D. is supported by the Spanish Research Project PSI2016-75688-P (AEI/FEDER, EU), by the European Union's Horizon 2020 Research and Innovation Programme under grant agreements n. 720270 (HBP SGA1) and n. 785907 (HBP SGA2), and by the Catalan AGAUR Programme 2017 SGR 1545. MLK is supported by the ERC Consolidator Grant: CAREGIVING (n. 615539), Center for Music in the Brain, funded by the Danish National Research Foundation (DNRF117), and Centre for Eudaimonia and Human Flourishing funded by the Pettit and Carlsberg Foundations.

References

Abraham, Alexandre, Michael P. Milham, Adriana Di Martino, R. Cameron Craddock, Dimitris Samaras, Bertrand Thirion, and Gael Varoquaux. 2017. "Deriving Reproducible Biomarkers from Multi-Site Resting-State Data: An Autism-Based Example." *NeuroImage* 147 (February): 736–45. https://doi.org/10.1016/j.neuroimage.2016.10.045.

Achard, Sophie, Raymond Salvador, Brandon Whitcher, John Suckling, and Ed Bullmore. 2006. "A Resilient, Low-Frequency, Small-World Human Brain Functional Network with Highly Connected Association Cortical Hubs." *The Journal of Neuroscience: The Official Journal of the Society for Neuroscience* 26 (1): 63–72. https://doi.org/10.1523/JNEUROSCI.3874-05.2006.

Arslan, Salim, Sofia Ira Ktena, Antonios Makropoulos, Emma C. Robinson, Daniel Rueckert, and Sarah Parisot. 2018. "Human Brain Mapping: A Systematic Comparison of Parcellation Methods for the Human Cerebral Cortex." *NeuroImage* 170 (April): 5–30. https://doi.org/10.1016/j.neuroimage.2017.04.014.

Dadi, Kamalaker, Mehdi Rahim, Alexandre Abraham, Darya Chyzhyk, Michael Milham, Bertrand Thirion, Gaël Varoquaux, and Alzheimer's Disease Neuroimaging Initiative. 2019. "Benchmarking Functional Connectome-Based Predictive Models for Resting-State FMRI." *NeuroImage* 192: 115–34. https://doi.org/10.1016/j.neuroimage.2019.02.062.

Deco, Gustavo, Josephine Cruzat, and Morten L. Kringelbach. 2019. "Brain Songs Framework Used for Discovering the Relevant Timescale of the Human Brain." *Nature Communications* 10 (1): 583. https://doi.org/10.1038/s41467-018-08186-7.

Deco, Gustavo, Morten L. Kringelbach, Viktor K. Jirsa, and Petra Ritter. 2017. "The Dynamics of Resting Fluctuations in the Brain: Metastability and Its Dynamical Cortical Core." *Scientific Reports* 7 (1): 3095. https://doi.org/10.1038/s41598-017-03073-5.

Deco, Gustavo, Adrián Ponce-Alvarez, Patric Hagmann, Gian Luca Romani, Dante Mantini, and Maurizio Corbetta. 2014. "How Local Excitation–Inhibition Ratio Impacts the Whole Brain Dynamics." *The Journal of Neuroscience* 34 (23): 7886–98. https://doi.org/10.1523/JNEUROSCI.5068-13.2014.

Geniesse, Caleb, Olaf Sporns, Giovanni Petri, and Manish Saggar. 2019. "Generating Dynamical Neuroimaging Spatiotemporal Representations (DyNeuSR) Using Topological Data Analysis." *Network Neuroscience* 3 (3): 763–78. https://doi.org/10.1162/netn_a_00093.

Glasser, Matthew F., Stamatios N. Sotiropoulos, J. Anthony Wilson, Timothy S. Coalson, Bruce Fischl, Jesper L. Andersson, Junqian Xu, et al. 2013. "The Minimal Preprocessing Pipelines for the Human Connectome Project." *NeuroImage* 80 (October): 105–24. https://doi.org/10.1016/j.neuroimage.2013.04.127.

Glerean, Enrico, Juha Salmi, Juha M. Lahnakoski, Iiro P. Jääskeläinen, and Mikko Sams. 2012. "Functional Magnetic Resonance Imaging Phase Synchronization as a Measure of Dynamic Functional Connectivity." *Brain Connectivity* 2 (2): 91–101. https://doi.org/10.1089/brain.2011.0068.

Hagmann, Patric, Leila Cammoun, Xavier Gigandet, Reto Meuli, Christopher J. Honey, Van J. Wedeen, and Olaf Sporns. 2008. "Mapping the Structural Core of Human Cerebral Cortex." *PLOS Biology* 6 (7): e159. https://doi.org/10.1371/journal.pbio.0060159.

Hilger, Kirsten, Makoto Fukushima, Olaf Sporns, and Christian J. Fiebach. 2020. "Temporal Stability of Functional Brain Modules Associated with Human Intelligence." *Human Brain Mapping* 41 (2): 362–72. https://doi.org/10.1002/hbm.24807.

Horn, Andreas, Ningfei Li, Till A. Dembek, Ari Kappel, Chadwick Boulay, Siobhan Ewert, Anna Tietze, et al. 2018. "Lead-DBS v2: Towards a Comprehensive Pipeline for Deep Brain Stimulation Imaging." *NeuroImage* 184 (September): 293–316. https://doi.org/10.1016/j.neuroimage.2018.08.068.

Horn, Andreas, Martin Reich, Johannes Vorwerk, Ningfei Li, Gregor Wenzel, Qianqian Fang, Tanja Schmitz-Hübsch, et al. 2017. "Connectivity Predicts Deep Brain Stimulation

425 Outcome in Parkinson Disease." *Annals of Neurology* 82 (1): 67–78.
426 https://doi.org/10.1002/ana.24974.
427 Ji, Jie Lisa, Marjolein Spronk, Kaustubh Kulkarni, Grega Repovš, Alan Anticevic, and Michael
428 W. Cole. 2019. "Mapping the Human Brain's Cortical-Subcortical Functional Network
429 Organization." *NeuroImage* 185 (January): 35–57.
430 https://doi.org/10.1016/j.neuroimage.2018.10.006.
431 Jutten, Christian, and Jeanny Herault. 1991. "Blind Separation of Sources, Part I: An Adaptive
432 Algorithm Based on Neuromimetic Architecture." *Signal Processing* 24 (1): 1–10.
433 https://doi.org/10.1016/0165-1684(91)90079-X.
434 Lopes-dos-Santos, Vítor, Sidarta Ribeiro, and Adriano B.L. Tort. 2013. "Detecting Cell
435 Assemblies in Large Neuronal Populations." *Journal of Neuroscience Methods* 220 (2):
436 149–66. https://doi.org/10.1016/j.jneumeth.2013.04.010.
437 Mai, Anh-Thu, Tijl Grootswagers, and Thomas A. Carlson. 2019. "In Search of Consciousness:
438 Examining the Temporal Dynamics of Conscious Visual Perception Using MEG Time-
439 Series Data." *Neuropsychologia* 129 (June): 310–17.
440 https://doi.org/10.1016/j.neuropsychologia.2019.04.015.
441 Marčenko, V.A., and Leonid Pastur. 1967. "Distribution of Eigenvalues for Some Sets of
442 Random Matrices." *Math USSR Sb* 1 (January): 457–83.
443 McDonald, Amalia R., Jordan Muraskin, Nicholas T. Van Dam, Caroline Froehlich, Benjamin
444 Puccio, John Pellman, Clemens C. C. Bauer, et al. 2017. "The Real-Time FMRI
445 Neurofeedback Based Stratification of Default Network Regulation Neuroimaging Data
446 Repository." *NeuroImage* 146: 157–70.
447 https://doi.org/10.1016/j.neuroimage.2016.10.048.
448 Messé, Arnaud. 2019. "Parcellation Influence on the Connectivity-Based Structure–Function
449 Relationship in the Human Brain." *Human Brain Mapping* n/a (n/a).
450 https://doi.org/10.1002/hbm.24866.
451 Nooner, Kate Brody, Stanley J. Colcombe, Russell H. Tobe, Maarten Mennes, Melissa M.
452 Benedict, Alexis L. Moreno, Laura J. Panek, et al. 2012. "The NKI-Rockland Sample:
453 A Model for Accelerating the Pace of Discovery Science in Psychiatry." *Frontiers in*
454 *Neuroscience* 6 (October). https://doi.org/10.3389/fnins.2012.00152.
455 Peyrache, Adrien, Karim Benchenane, Mehdi Khamassi, Sidney I. Wiener, and Francesco P.
456 Battaglia. 2010. "Principal Component Analysis of Ensemble Recordings Reveals Cell
457 Assemblies at High Temporal Resolution." *Journal of Computational Neuroscience* 29
458 (1): 309–25. https://doi.org/10.1007/s10827-009-0154-6.
459 Proix, Timothée, Andreas Spiegler, Michael Schirner, Simon Rothmeier, Petra Ritter, and
460 Viktor K. Jirsa. 2016. "How Do Parcellation Size and Short-Range Connectivity Affect
461 Dynamics in Large-Scale Brain Network Models?" *NeuroImage* 142 (November): 135–
462 49. https://doi.org/10.1016/j.neuroimage.2016.06.016.
463 Salti, Moti, Simo Monto, Lucie Charles, Jean-Remi King, Lauri Parkkonen, and Stanislas
464 Dehaene. 2015. "Distinct Cortical Codes and Temporal Dynamics for Conscious and
465 Unconscious Percepts." *ELife* 4 (May). https://doi.org/10.7554/eLife.05652.
466 Schaefer, Alexander, Ru Kong, Evan M. Gordon, Timothy O. Laumann, Xi-Nian Zuo, Avram J.
467 Holmes, Simon B. Eickhoff, and B. T. Thomas Yeo. 2018. "Local-Global Parcellation of
468 the Human Cerebral Cortex from Intrinsic Functional Connectivity MRI." *Cerebral*
469 *Cortex* 28 (9): 3095–3114. https://doi.org/10.1093/cercor/bhx179.
470 Setsompop, K., R. Kimmlingen, E. Eberlein, T. Witzel, J. Cohen-Adad, J. A. McNab, B. Keil, et
471 al. 2013. "Pushing the Limits of in Vivo Diffusion MRI for the Human Connectome
472 Project." *NeuroImage* 80 (October): 220–33.
473 https://doi.org/10.1016/j.neuroimage.2013.05.078.
474 Stephan, Klaas Enno, Nikolaus Weiskopf, Peter M. Drysdale, Peter A. Robinson, and Karl J.
475 Friston. 2007. "Comparing Hemodynamic Models with DCM." *NeuroImage* 38 (3): 387–
476 401. https://doi.org/10.1016/j.neuroimage.2007.07.040.
477 Stitt, Iain, Karl J. Hollensteiner, Edgar Galindo-Leon, Florian Pieper, Eva Fiedler, Thomas
478 Stieglitz, Gerhard Engler, Guido Nolte, and Andreas K. Engel. 2017. "Dynamic
479 Reconfiguration of Cortical Functional Connectivity across Brain States." *Scientific*
480 *Reports* 7 (1): 1–14. https://doi.org/10.1038/s41598-017-08050-6.

Tagliazucchi, Enzo, Pablo Balenzuela, Daniel Fraiman, and Dante R. Chialvo. 2012. "Criticality in Large-Scale Brain FMRI Dynamics Unveiled by a Novel Point Process Analysis." *Frontiers in Physiology* 3: 15. https://doi.org/10.3389/fphys.2012.00015.

Van Essen, David C., Stephen M. Smith, Deanna M. Barch, Timothy E. J. Behrens, Essa Yacoub, and Kamil Ugurbil. 2013. "The WU-Minn Human Connectome Project: An Overview." *NeuroImage*, Mapping the Connectome, 80 (October): 62–79. https://doi.org/10.1016/j.neuroimage.2013.05.041.

Wong, K.-F. 2006. "A Recurrent Network Mechanism of Time Integration in Perceptual Decisions." *Journal of Neuroscience* 26 (4): 1314–28. https://doi.org/10.1523/JNEUROSCI.3733-05.2006.

Wutz, Andreas, Nathan Weisz, Christoph Braun, and David Melcher. 2014. "Temporal Windows in Visual Processing: 'Prestimulus Brain State' and 'Poststimulus Phase Reset' Segregate Visual Transients on Different Temporal Scales." *The Journal of Neuroscience* 34 (4): 1554–65. https://doi.org/10.1523/JNEUROSCI.3187-13.2014.

Figures

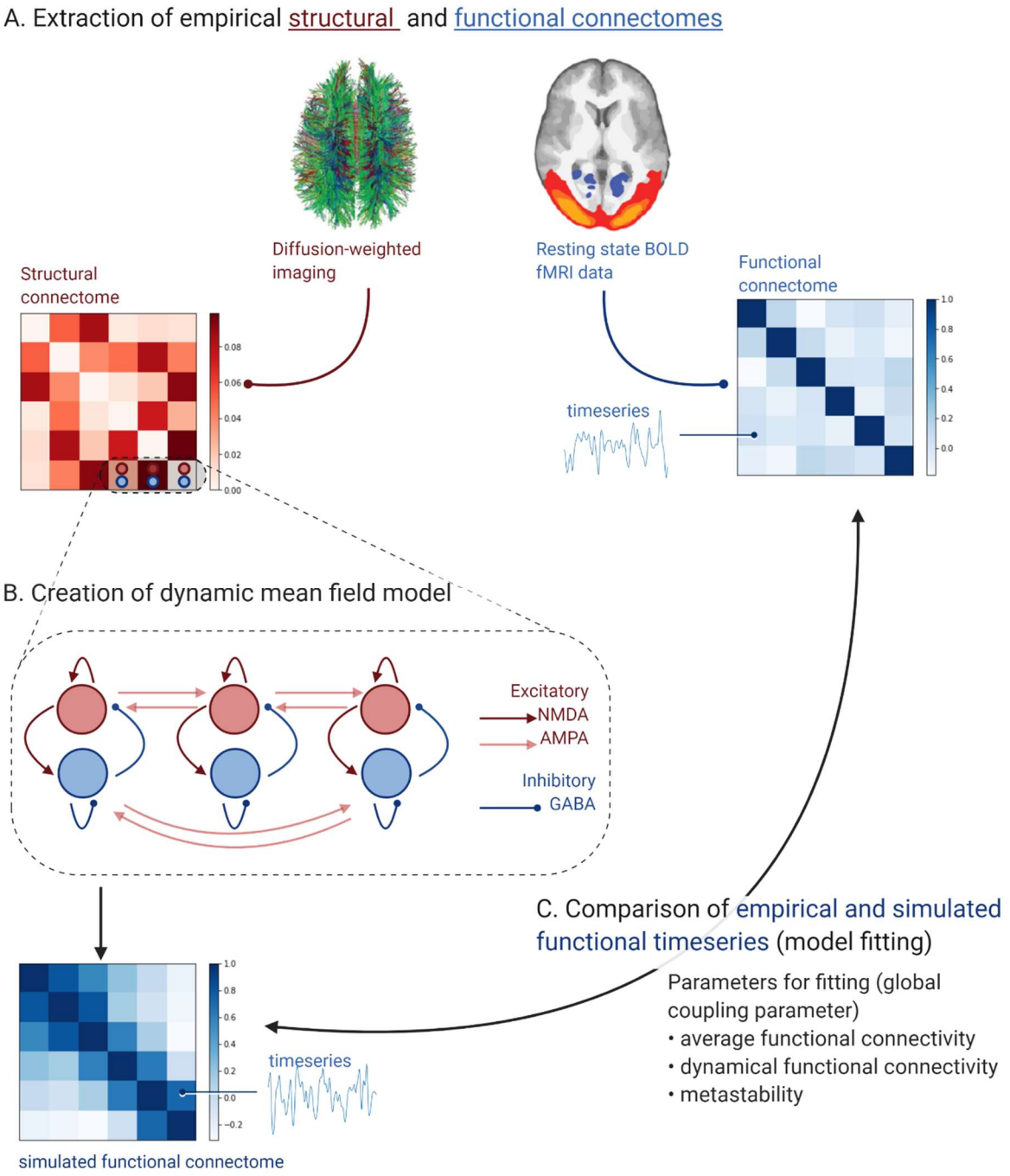

Figure 1. Whole-brain modelling steps to create functional timeseries in different temporal scales from empirical BOLD data. A. Extraction of BOLD timeseries from fMRI data and creation of structural connectome from diffusion-weighted data. B. Whole brain modelling of the excitatory and inhibitory neuronal sub-populations, taking into account the connections between regions through the weights of the structural connectome. C. Fitting the simulated functional timeseries to the empirical functional timeseries using metrics of average functional connectivity, Kuramoto synchronization index and dynamical functional connectivity.

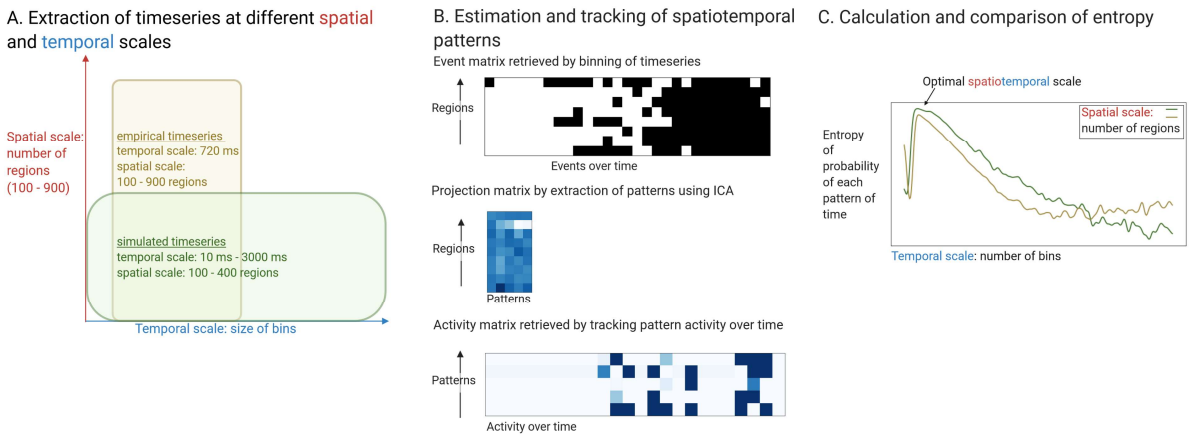

Figure 2. Extraction of spatiotemporal networks at different spatial and temporal scales. A. Extraction of a fixed temporal scale (given by TR) but different spatial scale of the empirical BOLD data and varying temporal scales (from milliseconds to seconds) of the simulated neuronal data. B. Binning of timeseries to create events over time, estimation of networks within data using ICA. Tracking of the resulting networks over time by projecting the event matrix onto the networks. C. Computation of the entropy of the activity of the networks as a function of their probability over time and comparison of the entropy across spatial and temporal scales.

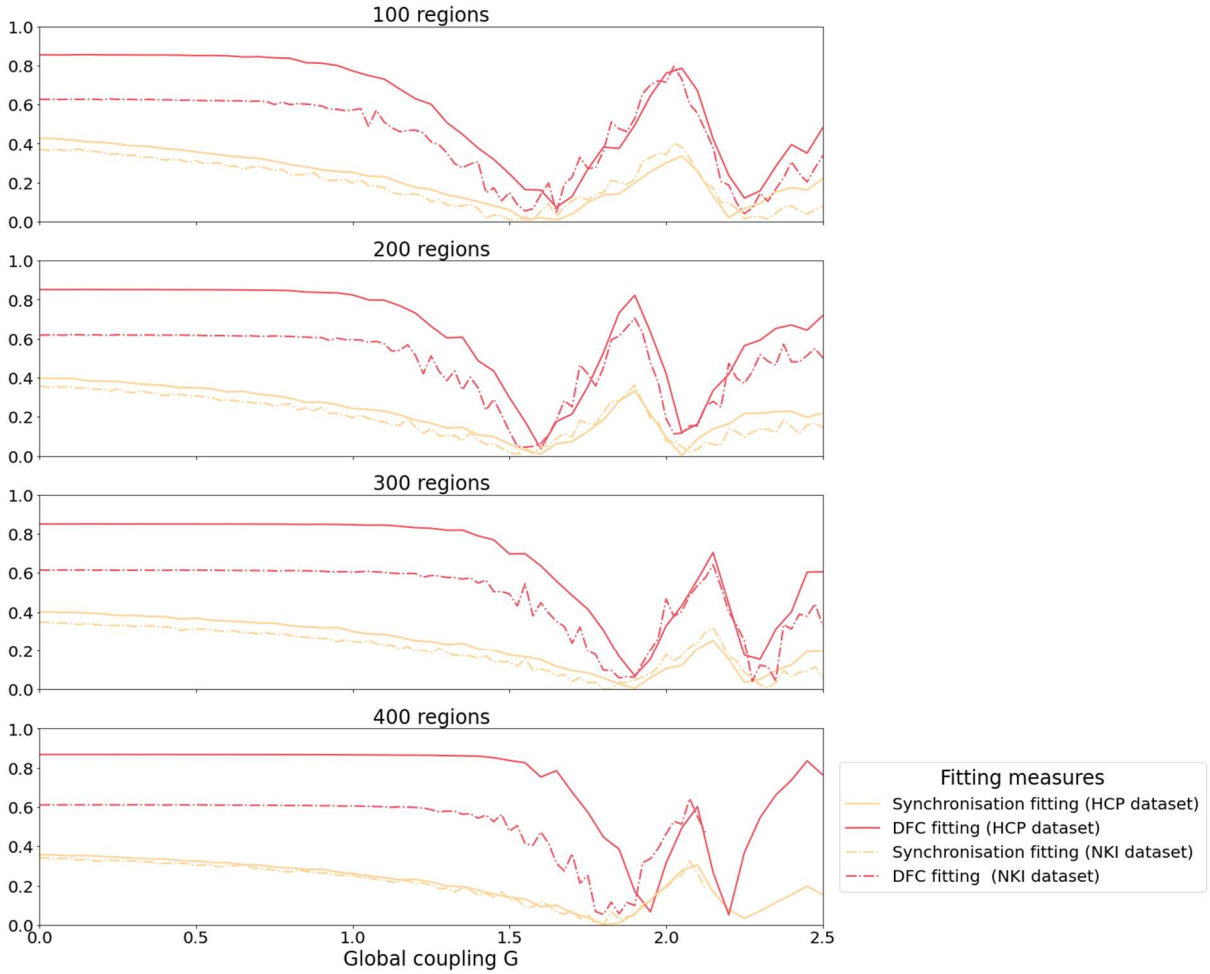

Figure 3. Fitting of the optimal working point of the model employing the global synchronization level and dynamical functional connectivity (DFC) across two independent datasets (HCP, NKI).

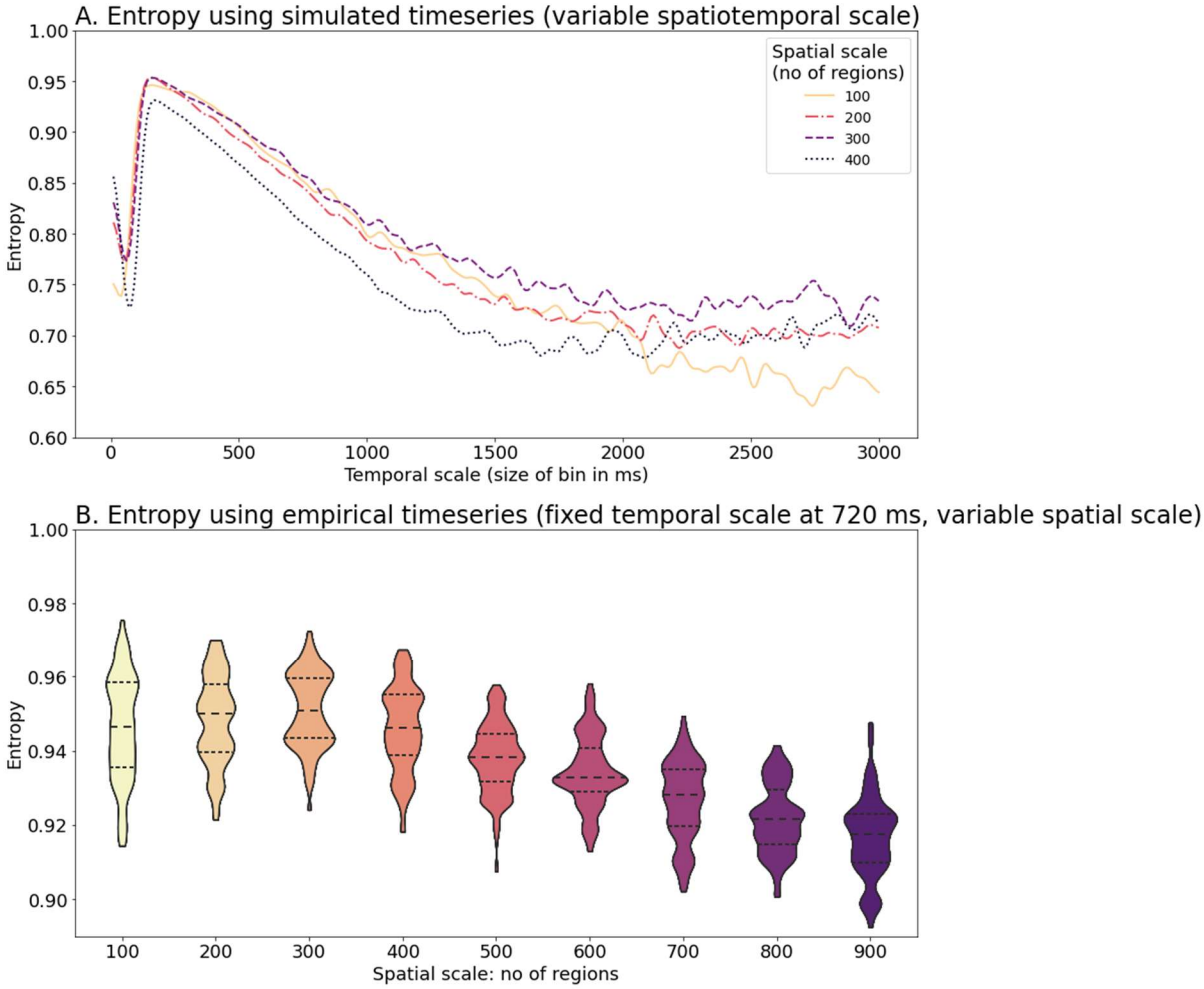

Figure 4. Entropy of temporal probability of spatiotemporal networks. A. Entropy using simulated timeseries with variable temporal scale with bin sizes from 10 to 3000 ms. The peak in the entropy shows a peak in the temporal scale of 200 ms and a spatial scale of 300 regions. There is clearly a decrease in entropy when using a scale of 400 regions.

B. Entropy using the empirical timeseries with a fixed temporal scale of 720 ms. The entropy follows an inverted U-shaped curve with a at 300 regions with only minor decreases at 100-400 regions, but with a marked decrease at spatial scales above 500 regions.

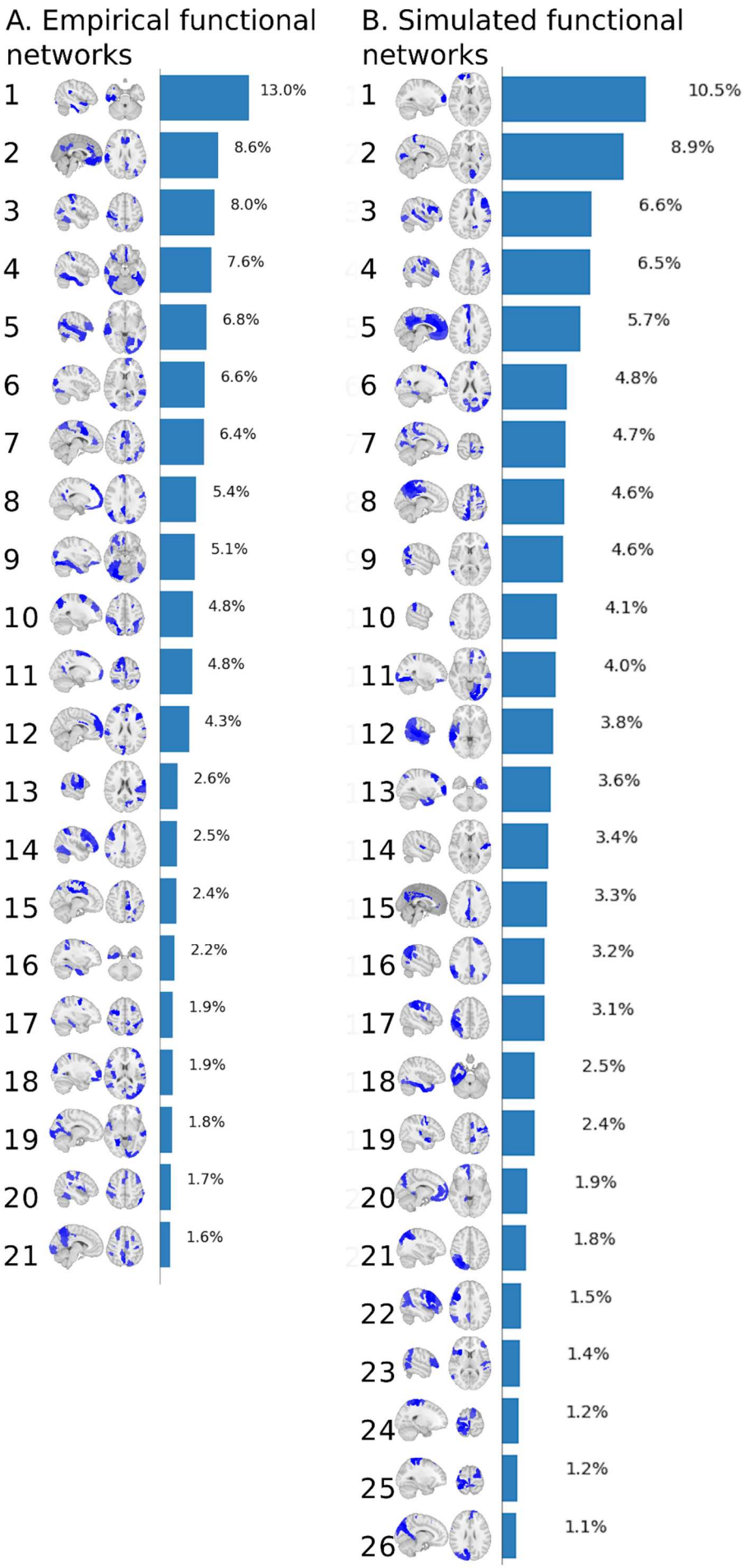

Figure 5. Spatiotemporal networks retrieved from empirical timeseries (A) and simulated timeseries at 200 ms (B) rendered on the standard brain and ordered by their probability of occurrence in percent.

Supplementary files

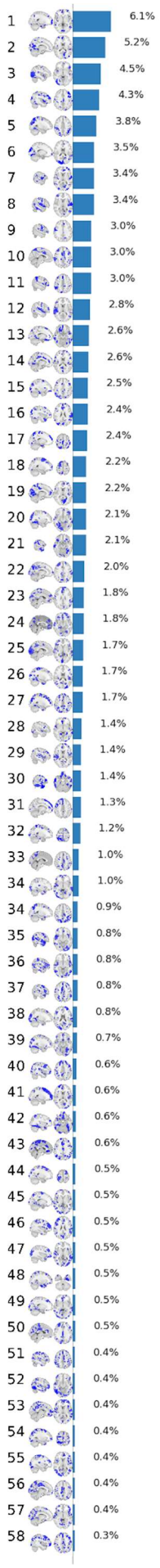

539 Figure S1. Empirical spatiotemporal networks at a spatial scale of n = 900 as derived with an
540 ICA and their probabilities of occurrence over time (in percent).
541